

# The synthesis of metoprolol monitored using Raman spectroscopy and chemometrics

Olof Svensson<sup>b</sup>, Mats Josefson<sup>a,\*</sup>, Frans W. Langkilde<sup>a</sup>

<sup>a</sup>Pharmaceutical Analytical R&D, AstraZeneca R&D, S-431 83 Mölndal, Sweden

<sup>b</sup>Department of Analytical and Marine Chemistry, Göteborg University, S-412 96 Göteborg, Sweden

Received 1 July 1999; received in revised form 21 February 2000; accepted 14 March 2000

## Abstract

The synthesis of Metoprolol base was studied using Raman spectroscopy with a 785-nm laser, optical fibres, a holographic transmission grating, confocal optics and a charge-coupled device (CCD) detector. The reaction mixture was heated according to a temperature gradient and spectra of the reaction mixture were obtained by focusing the laser beam through ordinary reaction flasks. Because of overlapping bands, multivariate techniques such as principal components analysis (PCA) and partial least-squares projections to latent structures (PLS) were used in the evaluation of the obtained spectra. The use of PCA or PLS against time does not require any calibration samples and a quantitative calibration is not necessary in order to monitor the reaction. A method for reaction endpoint determination, based on euclidean distances in the score space, is presented. The use of multivariate batch control charts have been demonstrated and a number of problems and solutions regarding the sample presentation have been discussed. The effect of spectral pretreatment on the multivariate results is shown and discussed. The monitoring results show that the time to produce Metoprolol base could be reduced. © 2000 Elsevier Science B.V. All rights reserved.

**Keywords:** Raman; Chemometrics; Multivariate analysis; Reaction monitoring; Batch control charts; Principal components analysis; PCA; Partial least-squares; PLS

## 1. Introduction

The use of new and rapid instrumentation in Raman spectroscopy has made the technique suitable for process monitoring. A number of liquid and solid-state reactions and processes have been studied (Barrie and Aitchison, 1992; Larsen et al., 1993; Vorsina et al., 1995; Nelson and Scranton, 1996; Rice et al., 1996; Schoppelrei et al., 1996; van Staden et al., 1996) by Raman spectroscopy using laser wavelengths ranging from 496 to 1064 nm. The use of short wavelengths may cause problems with fluorescence, and measurements in the near infrared region can be a problem when studying heated processes (Schoppelrei et al., 1996).

Optical fibres (Chong et al., 1992; Vickers and Mann, 1992; Wang et al., 1992; Ford et al., 1994; Nave et al., 1995; Al-Khanbashi et al., 1996) in combination with charge-coupled device (CCD) detectors can be used to

record several Raman spectra simultaneously (Vess and Angel, 1992; Marteau et al., 1994a,b; Pelletier et al., 1996). Optical fibres also allow remote monitoring (Farquharson and Simpson, 1992; Purcell et al., 1992; Martin et al., 1993; Marteau et al., 1995) of processes in hostile environments.

Principal components analysis (PCA) and partial least-squares/projections to latent structures (PLS) are common multivariate methods when using near infrared spectroscopy (NIR), but in Raman spectroscopy multivariate methods are not used to the same extent as in NIR. In Raman spectroscopy the bands often are sharp and selective, while NIR spectra typically have broad, unselective bands. This is the main reason why it is easier to use univariate methods in Raman spectroscopy than in NIR. In a recent paper, we showed that in a simple case with selective peaks, Raman spectroscopy in combination with multivariate methods such as PCA and PLS will give the same results as Raman spectroscopy and univariate methods based on peak heights or peak areas (Svensson et al., 1999). However, when several large and similar molecules are used in a reaction mixture, the Raman spectrum

\*Corresponding author. Tel.: +46-31-776-1658; fax: +46-31-776-3813.

E-mail address: mats.josefson@astrazeneca.com (M. Josefson)

becomes more complex, and the Raman bands will overlap each other. In such cases, it is preferable to use multivariate methods like PCA and PLS, because they do not require selective bands. When multivariate methods are used in Raman spectroscopy, they are mainly used for quantitative calibration purposes (Seasholtz et al., 1989; Williams et al., 1990; Aust et al., 1997; Cooper et al., 1997; Delgado-Lopez, 1997; Shimoyama et al., 1997).

In the pharmaceutical industry almost all processes are performed as batch processes, therefore multivariate methods for batch process monitoring and control are important. Multivariate methods based on unfolding of the three-dimensional matrixes obtained in batch process monitoring have recently been developed (Nomikos and MacGregor, 1994, 1995a,b; Rännar et al., 1998; Wold et al., 1998).

The objective of this paper is to show that Raman spectroscopy in combination with chemometric methods such as PCA and PLS can be used to monitor a process, in this case the synthesis of Metoprolol base, without the need for quantitative calibrations.

## 2. Theoretical methods

In the following sections, the matrix  $\mathbf{X}$  is made up from  $n$  rows and  $k$  columns, where each row represents a spectrum and each column represents one wavenumber (or wavelength). When partial least-squares regression (PLS) is used, a vector containing the local batch time is used as  $\mathbf{y}$ . The  $\mathbf{X}$  matrix and the  $\mathbf{y}$  vector have the same number of rows, which means that for each time in  $\mathbf{y}$  a spectrum in  $\mathbf{X}$  was measured.

### 2.1. Spectral pretreatment

The multivariate analysis was performed on spectra subjected to the standard normal variate transform (SNV) (Barnes et al., 1989; Dhanoa et al., 1994). The SNV transform is a preprocessing technique used to correct spectra for additive and multiplicative effects. The transformation is done on each spectrum individually by subtracting the spectrum mean and scaling with the spectrum standard deviation according to

$$\mathbf{x}_{i,\text{SNV}} = \frac{(\mathbf{x}_i - \bar{x})}{\sqrt{\frac{\sum_{i=1}^k (\mathbf{x}_i - \bar{x})^2}{k-1}}} \quad (1)$$

where  $\mathbf{x}_{i,\text{SNV}}$  is the transformed Raman intensity for wavenumber  $\mathbf{x}_i$ , and  $\bar{x}$  is the mean intensity of all the  $k$  wavenumbers in the spectrum. Eq. (1) shall be repeated for all  $k$  wavenumbers in the spectrum. Effectively, the operation is centering and normalizing the rows. In addition to the SNV transformation the standard column

centering was performed before applying principal component analysis or partial least-squares regression.

One advantage with SNV is that there is no need to store any values for future transformations, as is the case with multiplicative signal correction (MSC) (Dhanoa et al., 1994).

### 2.2. Principal components analysis (PCA)

Principal components analysis is a projection method which projects, in this case, spectra as points in a space with a small number of principal components. The principal components are extracted from the  $\mathbf{X}$  matrix in such a way that each principal component (PC) explains as much of the variation in  $\mathbf{X}$  as possible. In PCA, one PC consists of two vectors, one score vector  $\mathbf{t}$  and one loading vector  $\mathbf{p}$ . The score vector contains a score value for each spectrum, which tells how the spectrum is related to the other spectra in that particular PC. The loading vectors  $\mathbf{p}_a$  show spectral features, where high absolute values indicate a large influence on the PCA model.

The  $\mathbf{X}$  matrix can be expressed as

$$\mathbf{X} = \mathbf{t}_1\mathbf{p}'_1 + \mathbf{t}_2\mathbf{p}'_2 + \dots + \mathbf{t}_A\mathbf{p}'_A + \mathbf{E} \quad (2)$$

where  $A$  denotes the number of PCs extracted and  $\mathbf{E}$  is a residual matrix with the same number of rows and columns as  $\mathbf{X}$ .

The number of PCs to use can be determined by, for example, cross-validation (Wold, 1978). In process analytical applications, such as synthesis monitoring, the number of principal components usually is much smaller than the number of spectra ( $n$ ) and variables ( $k$ ).

### 2.3. Partial least-squares/projection to latent structures (PLS)

Partial least-squares (PLS) (Martens and Næs, 1989) is like PCA a projection method. The difference is that PLS is a regression method where a loading weight vector  $\mathbf{w}$  is used to extract as much variation in  $\mathbf{X}$  as possible, under the constraint that the variation extracted from  $\mathbf{X}$  is correlated with the variation in  $\mathbf{y}$ . This can be expressed as

$$\mathbf{w}_a = \frac{\mathbf{X}'_{a-1}\mathbf{y}_{a-1}}{\|\mathbf{X}'_{a-1}\mathbf{y}_{a-1}\|} \quad (3)$$

$$\mathbf{t}_a = \mathbf{X}_{a-1}\mathbf{w}_a \quad (4)$$

$$c_a = \frac{\mathbf{t}'_a\mathbf{y}_{a-1}}{\mathbf{t}'_a\mathbf{t}_a} \quad (5)$$

$$\mathbf{y} = c_1\mathbf{t}_1 + c_2\mathbf{t}_2 + \dots + c_A\mathbf{t}_A + \mathbf{f} \quad (6)$$

where  $a$  denotes PLS component number  $a$  and  $\mathbf{f}$  denotes the non-modelled variation in  $\mathbf{y}$ . The score vector  $\mathbf{t}_a$  can be interpreted in the same way as in PCA. The loading weight vectors  $\mathbf{w}_a$  show the spectral features in  $\mathbf{X}$  that best correlate with  $\mathbf{y}$ . High absolute values indicate a large

influence on the PLS-model. In this paper, time is used as  $y$ .

The number of PLS components to use can be estimated by cross-validation or an independent test set. When using PLS in batch control charts it is recommended to extract as many PLS components as necessary to explain at least 85% of the  $X$  matrix (Umetri, 1998).

#### 2.4. Batch control charts

When a batch process is monitored, a number of variables are measured at different times until the process has stopped. Then the same variables are measured for every batch produced. The situation is illustrated in Fig. 1A.

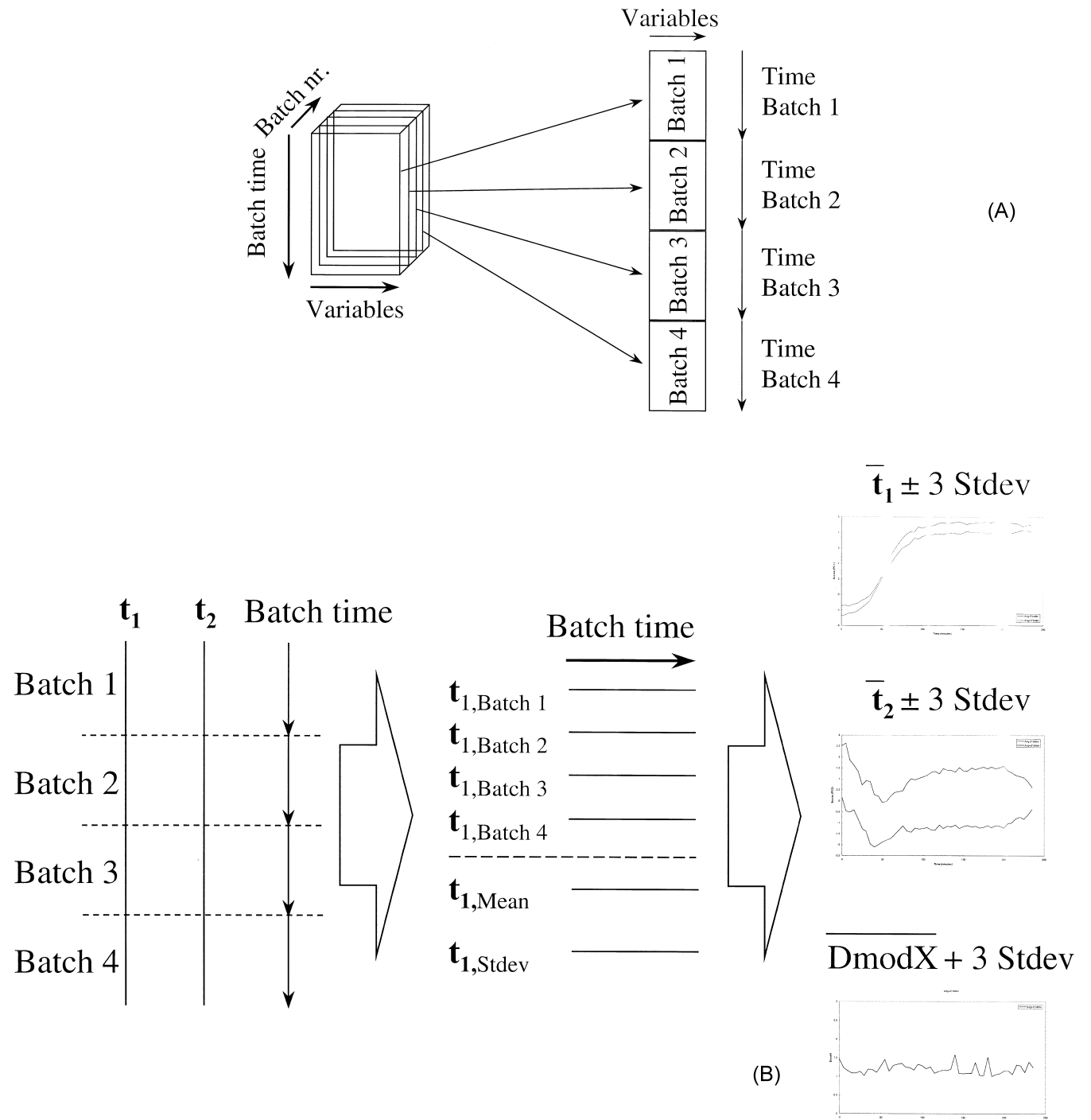


Fig. 1. (A) Batch data organized in a 3D matrix unfolded to a 2D matrix with batches placed under each other and local batch time increasing within each batch. Variables in columns. (B) Mean score value computed for each component individually at each local batch time, after PCA or PLS. Control charts for scores and distances to the  $X$  model ( $D_{\text{mod}X}$ ) for each PCA/PLS component plotted with mean  $\pm 3$  S.D.

One way to construct multivariate statistical process control (MSPC) charts for batch processes is to first unfold the 3D matrix. The unfolding can be done by placing the batches under each other according to Fig. 1A and then perform PCA or PLS on the unfolded matrix. When PLS is used, the local batch time or some kind of batch maturity variable, is used as a  $y$  vector.

The next step is to compute the mean score value for each PCA or PLS component, at all local batch times. The mean is computed over all batches. This step is illustrated in Fig. 1B. The standard deviation of the score values is computed according to the same principle as the mean.

The control limits are computed as the mean score values  $\pm$  a number of standard deviations, typically 2 or 3. This means that there is one control chart for each principal or PLS component, as shown in Fig. 1B.

The residuals from the PCA or PLS calculations can be used to calculate the distance for a certain observation (all variables measured at a specific time), to the model. The distance-to-model ( $D_{\text{mod}}X$ ) for a sample (spectrum)  $i$  included in the calibration can be computed according to

$$D_{\text{mod}}X_i = \sqrt{\frac{\sum_{j=1}^k e_{ij}^2}{k-A}} \cdot F \quad (7)$$

$$F = \sqrt{\frac{n}{n-A-1}} \quad (8)$$

where  $F$  is a correction factor used to take into account that the calibration samples have influenced the model. In Eqs. (7) and (8),  $A$  is the number of PCA/PLS components used in the batch process model,  $k$  is the number of variables in the samples (spectra), and  $n$  is the number of calibration samples. The  $D_{\text{mod}}X$  control chart is constructed by first calculating the mean  $D_{\text{mod}}X$  over all batches at each local batch time. Second, the standard deviation of  $D_{\text{mod}}X$  at each local batch time is computed. The last step is to compute the control limit as the mean  $D_{\text{mod}}X$  values + a number of standard deviations. This means that  $D_{\text{mod}}X$  control charts are constructed in the same way as for the scores (Fig. 1B), but with an upper limit only. For a new observation  $i$ , the distance to the model is computed as in Eq. (7), but without the correction factor  $F$ .

This way of unfolding the  $\mathbf{X}$  matrix and the use of separate control charts for scores and  $D_{\text{mod}}X$  in multivariate batch control and monitoring was recently developed by Wold et al. (1998). Classification and determination of final quality of a product was discussed by Thelin et al. (1995).

### 3. Experimental

#### 3.1. Raman spectrometer

A HoloProbe Raman spectrometer from Kaiser Optical

Systems (Ann Arbor, MI, USA) was used in all experiments in this paper. This spectrometer is equipped with a charge-coupled device (CCD) detector, which allows a full Raman spectrum to be collected in a few seconds, a holographic transmission grating, an optical fibre, and confocal optics which means that a Raman spectrum can be measured at different depths in a sample, or through ordinary glassware. The laser used was a 250-mW diode laser at 785 nm with adjustable laser power. In the present experiments, a laser power of approximately 100 mW was used. Spectra were collected between Raman shift 0 and 1959  $\text{cm}^{-1}$ , but only the part between 250 and 1959  $\text{cm}^{-1}$  was used in the evaluation of the data.

#### 3.2. Experimental set-up

An ordinary round-bottom flask with three bottlenecks was equipped with a reflux condenser, a temperature probe, and a propeller. The reaction vessel was then placed in a thermostat bath and a stirring motor was attached to the propeller.

The laser beam from the Raman instrument was focused on the reaction mixture, through the glass wall of the reaction vessel. The Raman probe head and the reaction vessel holder were kept in fixed positions during the design experiments, in order to avoid refocusing before the start of each Raman measurement series.

#### 3.3. Software

The HoloGRAMS ver. 3.0 software (Kaiser Optical Systems) was used to control the spectrometer. Spectra were exported to GRAMS/386 ver. 3.01 (Galactic Industries, Salem, NH, USA). The Grams file format was then used for import to The Unscrambler ver. 6.11b (Camo AS, Trondheim, Norway), MATLAB 5.2 (The Mathworks, Natick, MA, USA) and to SIMCA-P ver. 7.01 (Umetrics AB, Umeå, Sweden) for calculations. Modde 4.0 (Umetrics AB, Umeå, Sweden) was used for evaluation of the experimental design.

#### 3.4. Chemicals

Isopropanol (99.8%, Merck, Darmstadt, Germany), isopropylamine (>99.5%, Fluka Chemie, Buchs, Switzerland; 99%, Aldrich, Milwaukee, WI, USA; or 98–100%, Kebo, Stockholm, Sweden) and methoxy ethyl epoxy propoxy benzene (MEEP) (Astra, Södertälje, Sweden) were used in this study.

#### 3.5. Synthesis

The synthesis of Metoprolol base was performed by mixing MEEP and isopropylamine in isopropanol and then heat the reaction mixture applying a temperature

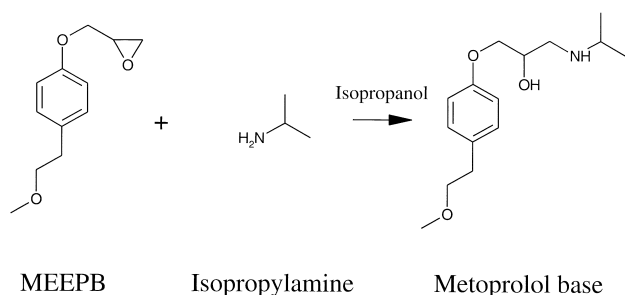


Fig. 2. Molecular structures for the synthesis of Metoprolol base.

gradient. The reaction scheme for the Metoprolol base synthesis is shown in Fig. 2.

### 3.6. Experimental procedure

According to the experimental design below, isopropanol and MEEPB were mixed in the reaction vessel and cooled to approximately 10°C in order to slow down the initial reaction rate and to simulate real synthesis conditions. According to the design, isopropylamine was added to the isopropanol/MEEPB mixture when the temperature in the reaction vessel was stable. After addition of isopropylamine the reaction vessel was closed, and a black curtain was placed over the fume hood in order to prevent changing daylight to influence the Raman spectra.

Next, the Raman measurements and the temperature measurements were started. The temperature was measured every minute, and every fifth minute a Raman spectrum was collected. The exposure time was 5 s for each spectrum.

After the first spectrum was measured, the temperature in the thermostat bath was adjusted according to the experimental design. Measurements were done for 4 h when using a fast temperature gradient and for 5 h when using a slow temperature gradient.

### 3.7. Experimental design

An introduction to experimental design can be found elsewhere (Box et al., 1978). The amount of isopropanol, isopropylamine and MEEPB was adjusted according to the  $2^{4-1}$  fractional factorial experimental design shown in Table 1. The experiments were performed in the order from A to L. Experiment B was added to the design in order to check the monitoring conditions for reactions with all factors, except the temperature gradient, set to low levels. Two different temperature gradients were used, one fast and one slow. The fast temperature gradient was achieved by changing the temperature in the thermostat bath (25, 40, 55, approximately 68°C), with a step every 15 min. The same temperatures were used to produce the slow temperature gradient, but the temperature was changed every hour instead of every 15 min.

Table 1  
Experimental design for the Metoprolol base synthesis<sup>a</sup>

Expt.	Propanol	MEEPB	Amine	Gradient	Estimated endpoint <sup>b</sup>
C	–	–	–	Slow	250
J	+	–	–	Fast	140
I	–	+	–	Fast	155
F	+	+	–	Slow	250
E	–	–	+	Fast	150
K	+	–	+	Slow	245
G	–	+	+	Slow	260
A	+	+	+	Fast	160
D	0	0	0	Fast	145
H	0	0	0	Fast	160
L	0	0	0	Fast	155
B	–	–	–	Fast	150

<sup>a</sup> High and low levels indicated with + and –, respectively.

<sup>b</sup> Estimated endpoint in minutes.

## 4. Results and discussion

### 4.1. Spectra

In Fig. 3, spectra from MEEPB, Metoprolol base, isopropanol and isopropylamine are shown. As can be seen from the spectra, there are overlapping bands in the whole spectral region. In Fig. 4, spectra from the reaction mixture are shown as the reaction proceeds. Decreasing spectral bands can be observed at 765, 1125–1175 and 1225–1275  $\text{cm}^{-1}$ . At 885  $\text{cm}^{-1}$  one increasing band can be observed.

By subtracting the first spectrum from the last spectrum, the changing spectral features can be seen and compared to the pure spectra of Metoprolol base and MEEPB, as in Fig. 5. The comparison to pure spectra is difficult due to overlapping bands and peak shifts in the reaction mixture.

Because of the broad and overlapping bands in the spectra it is difficult to use univariate methods such as peak height and peak area determinations to follow the reaction. However, if no other methods are available it may be possible to subtract the first spectrum from all other spectra, and get sharp bands to monitor. One drawback with this method is that it may be hard to find bands that are unaffected by band shifts and to find a stable baseline to compare with.

### 4.2. Multivariate evaluation of data based on single experiments

The results from PCA and PLS are quite similar and therefore figures are only shown for PCA data in this section. Two reactions will be shown, one with fast and one with slow temperature gradient.

Before further computations, the spectra were normalized with SNV. The 250–1959- $\text{cm}^{-1}$  region in the Raman spectra were used in the SNV calculations. This part of the spectra was also used for further evaluation. PCA or PLS

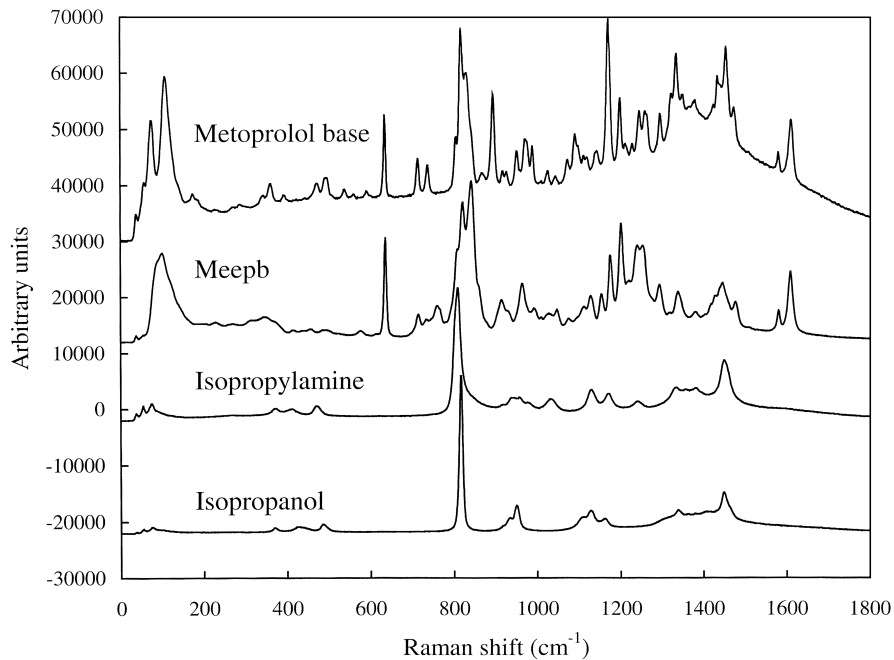


Fig. 3. From top to bottom: spectrum of pure Metoprolol base, MEEPb, isopropylamine and isopropanol (SNV-treated spectra).

was then applied to evaluate data from single experiments. In the PLS calculations the batch time was used as  $y$ .

In both the PCA and PLS results, after two PCA or PLS components  $R^2$  was between 95 and 98% for the spectral matrix in all experiments, except for two experiments where it was between 89 and 91%. The number of components to use was determined by looking at both the

$R^2$ ,  $Q^2$  and by checking the loading plots.  $R^2$  and  $Q^2$  do not improve after two components and the loading plot for the third component mainly contains high frequency noise. This is reasonable since the spectra mainly contain information about two things, the reaction and the temperature gradient. The temperature gradient and the scores for the first two components for one fast (A) and one slow (F)

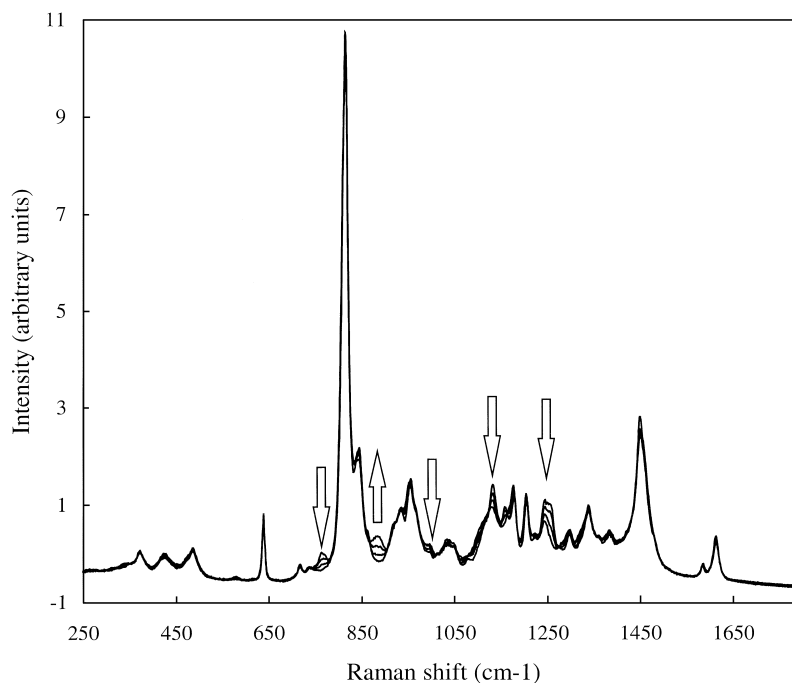


Fig. 4. Spectra from the reaction mixture after 0, 40, 60 and 240 min, respectively. Increasing and decreasing bands indicated by arrows.

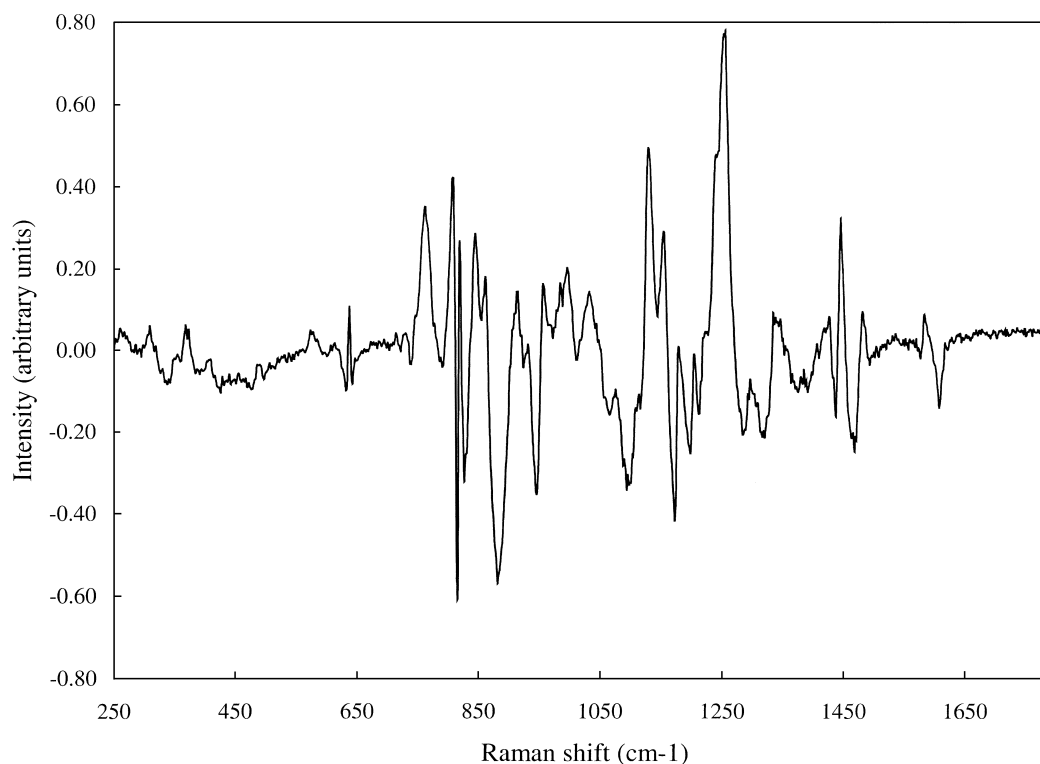


Fig. 5. Difference between the first and last spectrum for reaction A. Main spectral features changing during the reaction.

reaction, where A and F refer to order in the experimental design (Table 1), are shown in Fig. 6A and 6B, respectively.

The score trace for the first principal component (PC) shows the progress of the reaction. In the fast temperature gradient case, the reaction is slow in the beginning when the temperature is low and as the temperature increases, the reaction rate increases. The concentration change has its maximum where the slope of the score trace is largest. When the difference between two subsequent points in the score space is small, the reaction endpoint is reached. This means that when the score traces for the first components are approaching a constant level, the reaction is completed. The reaction endpoint was estimated as described below using two PCA components and is shown for all experiments in the design in Table 1.

An increase in the score trace for the first principal component may be observed at long reaction time in Fig. 6A. However, higher yield at longer reaction time may lead to higher amount of impurities. Moreover, a possible increase in the score trace may be due to evaporation of solvent.

In the case with a slow temperature gradient (Fig. 6B), at least three different reaction rates can be observed. The rate changes are seen as relatively sharp changes in the slope of the score trace. The reaction rate is slow at low temperatures and increases at higher temperatures. This is verified as the slope changes in the score trace for the first PC occur exactly as the temperature increases.

In the score trace for the second PC, changes in the temperature in combination with the reaction progress can be observed. In the fast gradient case, the score values increase as the temperature increases, and as the temperature becomes stable, the change in the trace is not due to change in temperature, but must be due to changes in the reaction mixture.

The slow gradient score trace for the second PC (Fig. 6B) shows a similar pattern as in the case with the fast gradient. The difference is that the pattern is repeated four times, because of the way the temperature was changed.

For the fast gradient experiment, the loading vectors for the first and second PC are shown in Fig. 7A and 7B, respectively. The loading vector for the first PC is difficult to compare to pure spectra due to the overlapping bands. However, a comparison between a spectrum computed as the difference between the first spectrum and the last spectrum in the reaction (Fig. 5), and the loadings for the first PC shows a strong similarity. Because the difference spectrum mainly reflects the synthesis of Metoprolol base, and the loading vector in the first PC is similar to this difference, the score trace for the first PC shows how the reaction proceeds. The loading vector seen for PC 2 in Fig. 7B may tentatively be assigned to contain contributions from band broadening and shifts brought about by the temperature change during the reaction.

Because the loadings for the slow gradient experiment are very similar to the loadings in Fig. 7, they are not shown. The loading and score plots for all experiments in

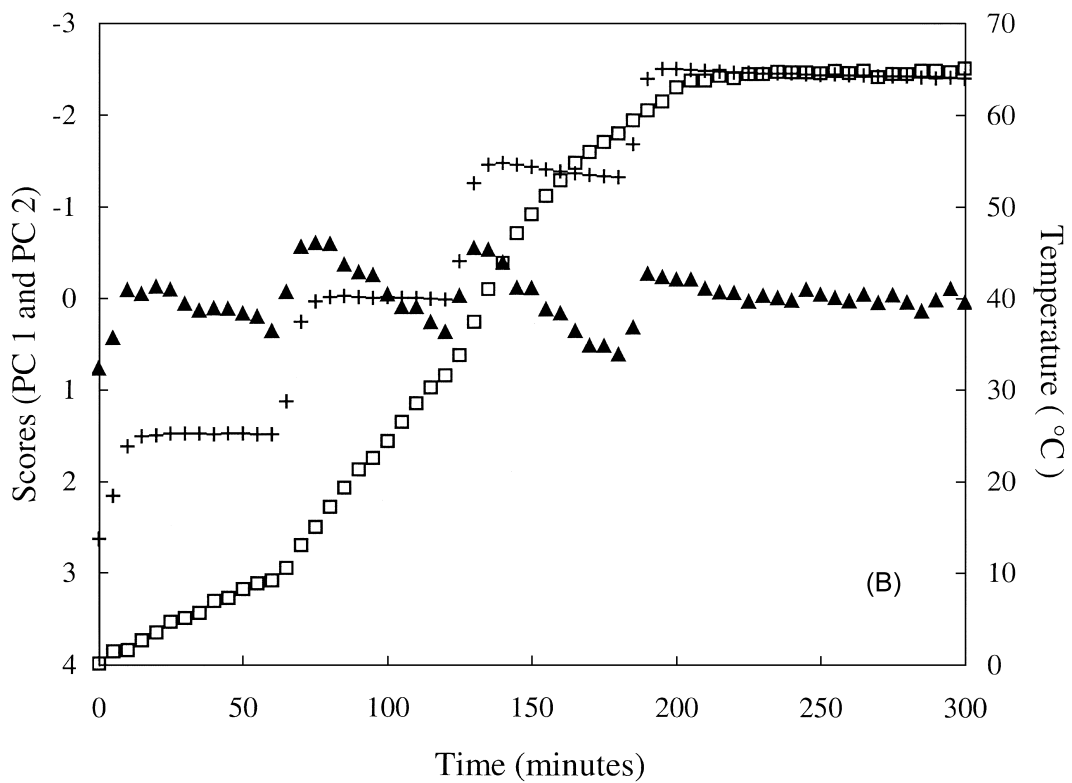
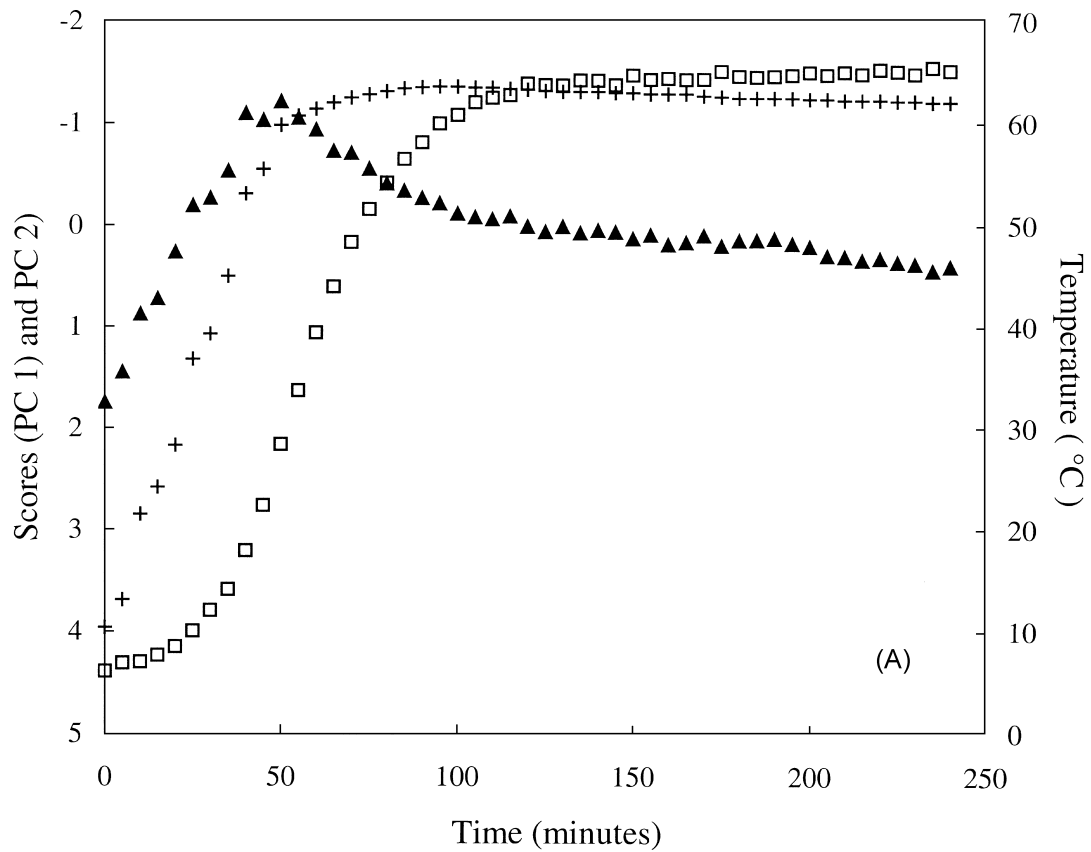


Fig. 6. Temperature in the reaction vessel (+) and score traces for the first ( $\square$ ) and second ( $\blacktriangle$ ) principal components. (A) Experiment A (fast) and (B) experiment F (slow temperature gradient). Abscissa, time (min); left ordinate, scores for PC 1 and 2; right ordinate, temperature in reaction vessel ( $^{\circ}\text{C}$ ).

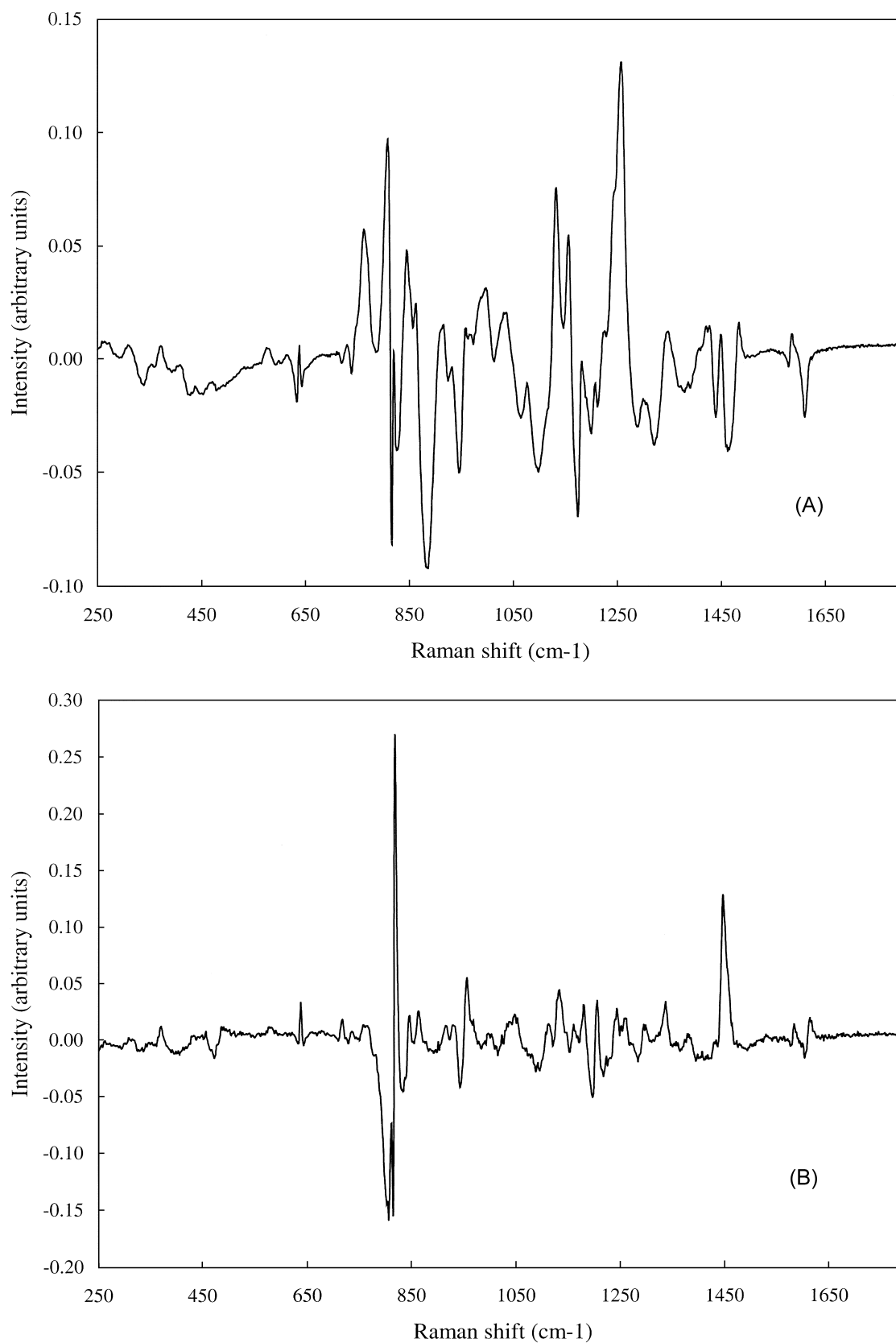


Fig. 7. Loadings for: (A) first PCA component, and (B) second PCA component, for reaction A.

the design are similar to those shown for the fast experiment A and the slow experiment F.

#### 4.3. Reaction endpoint determination

The reaction endpoint can be determined manually by looking at score plots for a number of PCA and PLS components. When the reaction score trace becomes stable and the distance between a number of subsequent spectra becomes small the reaction has reached its endpoint.

The endpoint determination described above can be done in a more objective way by calculation of the Euclidean distance between subsequent points, and when the distance has reached the noise level the reaction has reached its endpoint. These distances correspond to a multivariate measure of the reaction rate in a space spanned by the selected number of PCA or PLS components. In this paper the endpoint was determined in the following way.

First a PCA was performed on reaction L. Next, this model was applied on all spectra in each individual reaction. For two PCA components, the scores ( $s_i$ ) for each individual spectrum ( $i$ ) were used to calculate the Euclidean distance between spectra according to

$$s_i = [t_{1,i} \quad t_{2,i}] \quad (9)$$

$$d_i = \sqrt{(s_i - s_{i-1})(s_i - s_{i-1})'} \quad (10)$$

where  $t_{1,i}$  and  $t_{2,i}$  are the scores for spectrum  $i$  in PCA components 1 and 2, respectively,  $d_i$  is the distance between spectrum  $i$  and spectrum  $i-1$  in the score space,  $s_i$  is a row vector containing the scores for spectrum  $i$  and  $s_{i-1}$  contains the scores for spectrum  $i-1$ . In order to obtain a more stable distance measure, a moving average filter was applied to the computed distances according to

$$D_i = \frac{\sum_{j=0}^4 d_{i-j}}{5} \quad (11)$$

where  $D_i$  is the average distance for spectrum  $i$ . The derivative of these average distances was calculated as the difference between successive distances. The derivative was then smoothed by a moving average filter similar to Eq. (11). In order to keep a reasonably high resolution in time it was decided to use only five points for the smoothing. Because of the small number of points the Savitsky–Golay derivation was less stable than the moving average approach and therefore the latter was used in this case.

The endpoint limit was considered reached when the absolute value of the derivative was below 0.005, the temperature gradient had finished and the average distance between points was low. However, the limits can be adjusted depending on the problem. The above description of the endpoint determinations was performed by using

PCA scores, but the approach presented will work equally well with PLS scores. This endpoint determination can also be performed by updating the PCA or PLS model for each new spectrum measured. In the case with an updating model the approach becomes more sensitive to outliers. The results from the endpoint determinations are shown in Table 1.

It shall be noted that Raman spectroscopy has to be complemented by another analytical method for determination of impurities (detection limit ~0.1–1%). In this case it is also necessary with further validation of the endpoint time results found, since no reference measurements for yield and purities were performed.

In laboratory experiments similar to the ones performed in the present work, the yield of the synthesis was found to be above 90%, with purity above 99%.

#### 4.4. Evaluation of the experimental design

One of the objectives with this study was to investigate if it was possible to decrease the time for the synthesis of Metoprolol base and if different amounts of MEEP, isopropylamine and isopropanol would influence the reaction time. The design was evaluated in two different ways using multiple linear regression (MLR) with the reaction endpoint time as  $y$ . First, the whole  $2^{4-1}$  fractional factorial design in Table 1 was evaluated ( $R^2=0.99$  and  $Q^2=0.99$ ). In this type of design the main terms are confounded with three variable interaction terms and the two variable interaction terms are confounded with each other. In this first case where both slow and fast temperature gradient experiments were used in the evaluation of the design, the only significant factors were the two main terms, amount of MEEP and the temperature gradient. The sign of the MEEP coefficient was positive, which means that an increase in amount of MEEP will lead to an increase in reaction endpoint time. A slow temperature gradient will also increase the reaction endpoint time. This can also be seen by studying Table 1. The fact that temperature is important for the reaction can also be observed in Fig. 6A,B. In Fig. 6B it is obvious that the reaction rate changes with temperature. This shows that the temperature is important for the reaction endpoint, and therefore must be well controlled.

The actual process conditions are more similar to the fast temperature gradient case, and therefore a second evaluation was performed using only the fast temperature experiments. This results in a  $2^{3-1}$  fractional factorial design with three centerpoints and one additional experiment (B). In  $2^{3-1}$  fractional factorial designs the main terms are confounded with the two variable interaction terms. Using this design it is possible to determine if there are significant factors influencing the endpoint time of the reaction. In this second case when the design was evaluated with only fast temperature gradients, no significant

factors were found. This, in combination with the low model statistics ( $R^2=0.58$  and  $Q^2=0.16$ ), indicates that the endpoint time for the reaction is robust against changes within the design.

It can also be noted that if other responses such as yield and purity had been present, the reaction endpoint could have been used as an uncontrolled factor in the experimental design. However, in this case no further responses were measured.

#### 4.5. Use of multivariate batch control charts

The centerpoint experiments D, H and L were used together in one model for the multivariate batch control charts. The computations were performed using PLS with time as  $\mathbf{y}$ , and the control limits were determined as described in the theoretical methods section. The number of components was determined using  $R^2$ ,  $Q^2$  and by inspecting loading plots. The criterion that at least 85% of  $\mathbf{X}$  shall be explained was also used (see Section 2.3). The PLS model was based on three PLS components and  $R^2$  was 0.97 for the  $\mathbf{X}$  matrix and 0.74 for  $\mathbf{y}$ . One additional component can be expected in this case compared to the evaluation of a single reaction. In this case the third component explain the difference between the three centerpoints.

The PLS model described above was used to follow the evolution of the other reactions in the design. The control charts for the two first PLS components and the distance to the model for the fast corner experiments A, B, E, I and J are shown in Fig. 8A–C. In Fig. 8, 3 S.D. around the mean are shown. The control charts for PLS component 1 and  $D_{\text{mod}}X$  (Fig. 8A,C) show that all fast experiments at the corner points are outside the control limits in one or both charts. This verifies that deviating experimental conditions are detected in the batch control charts.

In Fig. 9 the first PLS component control chart for the slow experiments C, F, G and K is shown. The results show that by looking at the first component, in this case, it is possible to detect deviations in reaction speed. If this kind of deviations can be detected before the process is finished it should be possible for an operator to correct for them and get the process on the right track again.

An alternative way to introduce limits for a continuous process is to use the Hotellings  $T^2$  statistics to set the limits for allowed score values. In that case a common limit is set for all types of changes during the whole batch reaction, and will then be independent of the batch time. For a batch reaction, this type of time independent limits is less sensitive when small changes in the batch trace occur.

As described in the experimental section, the spectra were measured directly through the glass wall of the reaction vessel. One problem with this way of measuring the Raman spectra became clear when the batch control charts were used and new centerpoint reactions were performed. The new centerpoints were made several weeks

after the other experiments, and another reaction flask was used. The glass in the flask was not homogeneous, and hence the spectra became somewhat different from the previously measured ones. The use of a new batch of MEEPb, with a possible different purity, may also have contributed to the difference in the spectra. The result of this was that all new centerpoints were on or outside the control limits in the score control charts and definitely outside the control limits in the distance-to-model chart.

Problems which are related to the sample presentation (laser focus, vessel) should be possible to avoid in future experiments. One way to avoid problems with different reaction vessels would be to use some kind of immersion probe directly in the solution instead of measuring through the glass wall. Another way to deal with this problem would be to take the difference between all spectra and the first or an average of the first few spectra measured. This treatment should remove the differences that depend on different reaction vessels and different focus for each experiment. However, by using these differences it is not possible to tell if a new starting solution is different from previous starting solutions.

#### 4.6. Effects of spectral preprocessing

The SNV transform was used on all spectra in the above evaluation. In addition, the following spectral preprocessing methods were tested: multiplicative signal correction (MSC), range normalisation, first and second derivatives. The use of MSC or normalisation for spectral preprocessing gave similar score traces as with SNV, but the first and second derivatives gave somewhat different results.

The first PC score traces in Fig. 10A,B are based on second derivatives treated spectra from experiments A and F, respectively. These figures can be compared to Fig. 6A,B, which contain the same reactions but with SNV treated spectra. The score traces for second derivatives treated spectra follow the temperature gradient in both the fast and the slow temperature gradient cases, while the score traces for SNV treated spectra do not. The effect was the same for first derivatives but not as clear as for second derivatives. The score traces for the second PC behave in a similar way for both second derivatives and SNV treated spectra. This indicates that if a temperature gradient is present during a reaction or other process, the use of preprocessing methods such as SNV, MSC and normalisation should be preferred over first and second derivatives, if the main objective is to get a good picture of how the reaction proceeds. However, this does not mean that first and second derivatives automatically give different results compared to the other preprocessing methods, it only means that the information in the data is placed in different PCs or that the information is distributed over several PCs. The sensitivity of second derivatives spectra to temperature changes may be due to changes in band shapes and positions with temperature. The use of SNV may be seen

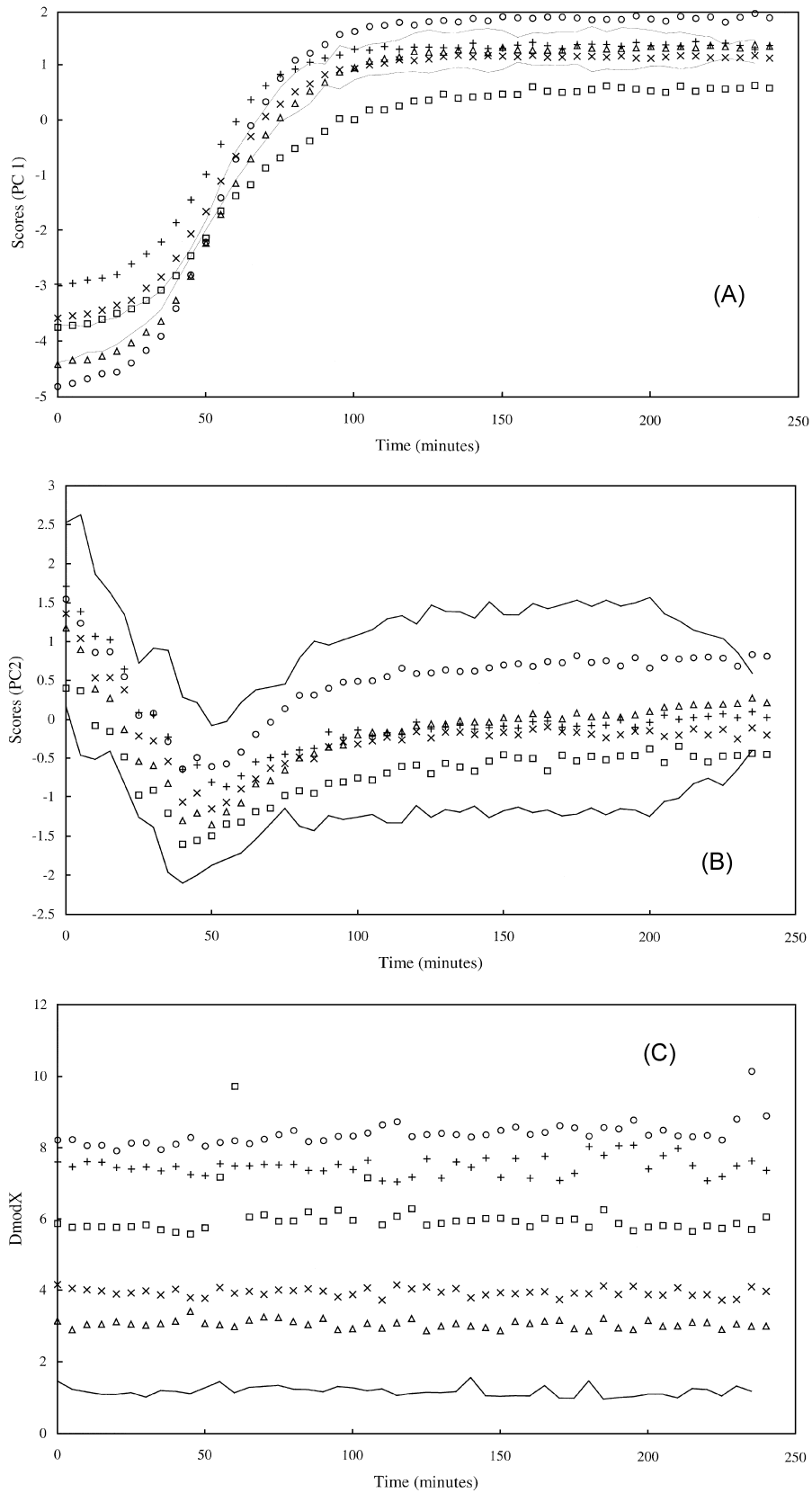


Fig. 8. Batch control charts for the reactions with fast temperature gradient: (A) first PLS component, (B) second PLS component and (C) distances to the  $X$  model ( $D_{\text{mod}X}$ ). Batch control model based on centerpoint reactions D, H and L. Reactions A ( $\Delta$ ), B ( $\times$ ), E ( $\square$ ), I ( $\circ$ ), and J ( $+$ ) shown in the control charts are all corner point reactions. Mean  $\pm 3$ S.D. indicated by lines. Centerpoint reactions not shown. Abscissa, time (min); ordinate, scores for PC 1, 2 and  $D_{\text{mod}X}$ , respectively.

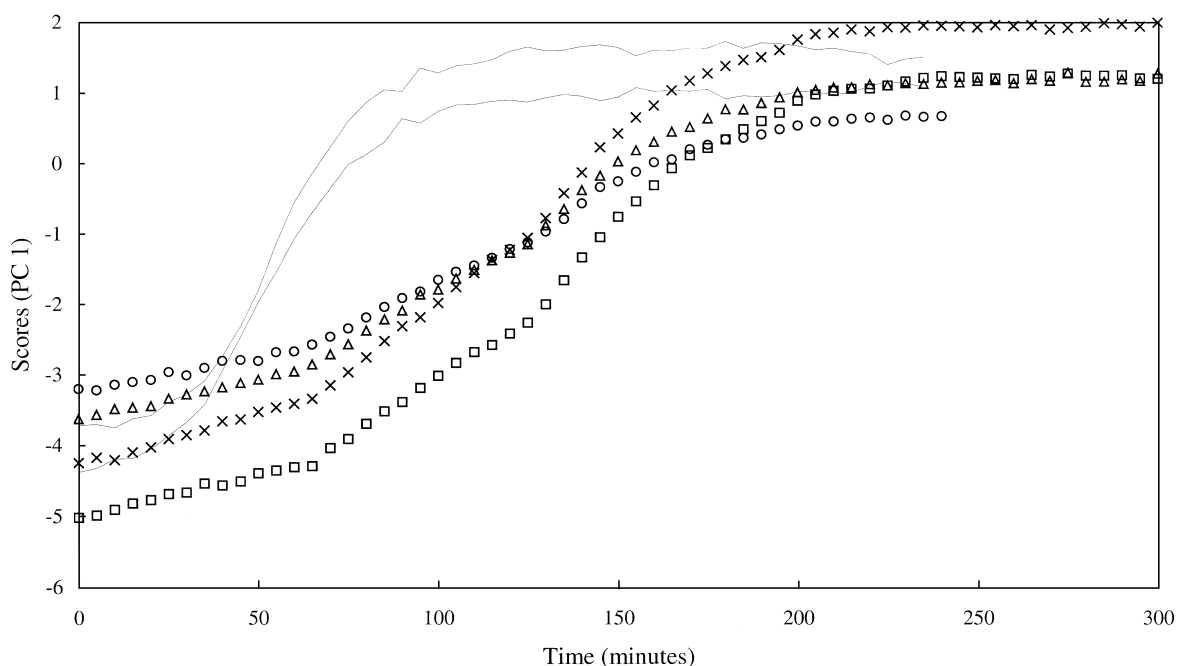


Fig. 9. Batch control chart for PLS component 1, for the reactions with slow temperature gradient (C ( $\Delta$ ), F ( $\times$ ), G ( $\square$ ) and K ( $\circ$ )). Mean  $\pm$  3\*S.D. indicated by lines. Batch control model based on centerpoint reactions D, H and L. Centerpoint reactions not shown. Abscissa, time (min); ordinate, scores for PC 1.

as a disadvantage because the score traces become more similar, but this is not a problem, since the difference from normal is clearly shown in the 'distance-to-model' plots (Fig. 8C), i.e., the information is still present but transferred from the model to the residuals.

## 5. Conclusions

A calibration free method for monitoring of organic syntheses, using Raman spectroscopy and PCA or PLS has been presented. The method does not require any quantitative determinations of concentrations and is therefore fast and easy to use. It should be possible to use this method even for unknown processes and reactions.

### 5.1. Reaction endpoint determinations

As part of the reaction monitoring, a method based on Euclidean distances in the score space, to determine if the reaction was finished, was presented. This method does not rely on concentration determinations and can therefore be useful also in unknown systems.

With further validation, the endpoint determination method could help decrease the reaction time without loss in yield. Since no final product was isolated and tested for yield and impurities, additional work must be performed in order to verify the results obtained. The test for impurities is important since Raman spectroscopy has a detection limit around 0.1–1%.

### 5.2. Experimental design

The results from the experimental design show that both the temperature gradient and the amount of MEEPB have a significant influence on the reaction endpoint time. However, when the design was evaluated for fast temperature gradients only, no significant factors were found.

### 5.3. Multivariate batch control charts

The use of multivariate batch control charts has been demonstrated. A number of problems with the sample presentation used have to be solved before the control charts can be used in a real situation. This can possibly be done by using an immersion probe instead of measuring through the glass wall of the reaction vessel, thus avoiding different focus for each new batch measured.

### 5.4. Effects of spectral pretreatment on the results

Depending on the spectral pretreatment, the information in the data may be located in different PCA or PLS components or will be distributed over several components. Therefore, depending on the purpose or type of reaction or process to monitor, different preprocessing methods can be used. In this case the chemical variation became more focused with SNV and MSC than with first and second derivatives.

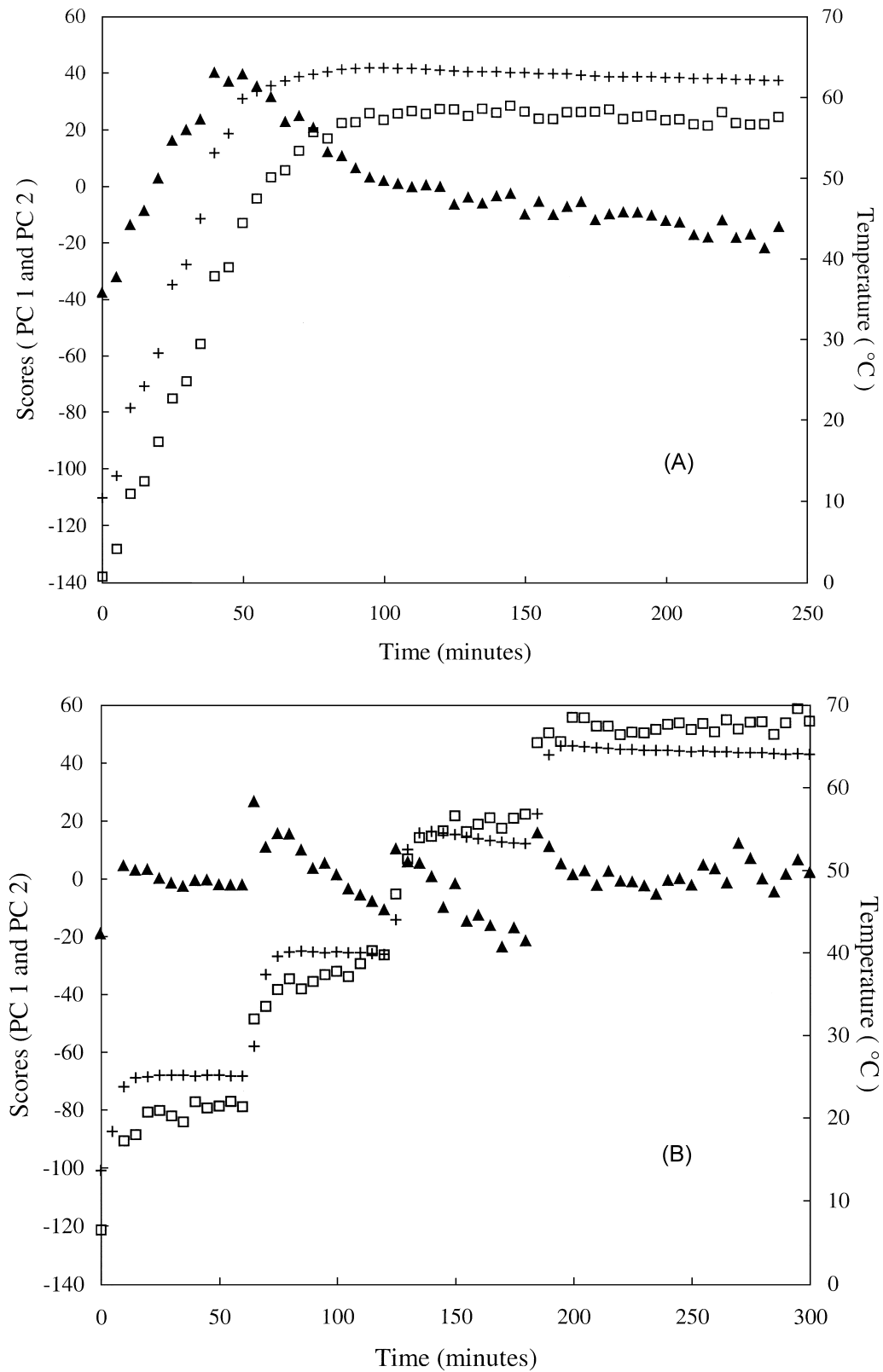


Fig. 10. Temperature in the reaction vessel (+) and score traces for the first (□) and second (▲) principal components. PCA model based on second derivative treated spectra. Compare to Fig. 6A,B. Abscissa, time (min); left ordinate, scores for PC 1 and 2; right ordinate, temperature in reaction vessel (°C). (A) Experiment A (fast) and (B) experiment F (slow temperature gradient).

## References

- Al-Khanbashi, A., Hansen, M.G., Wachter, E.A., 1996. Improved Fiber-Optic method for monitoring emulsion composition using Raman scattering. *Appl. Spectrosc.* 50, 1089–1092.
- Aust, J.F., Booksh, K.S., Stellman, C.M., Parnas, R.S., Myrick, M.L., 1997. Precise determination of percent cure of epoxide polymers and composites via fiber-optic Raman spectroscopy and multivariate analysis. *Appl. Spectrosc.* 51, 247–252.
- Barnes, R.J., Dhanoa, M.S., Lister, S.J., 1989. Standard Normal Variate transformation and de-trending of near-infrared diffuse reflectance spectra. *Appl. Spectrosc.* 43, 772–777.
- Barrie, J.D., Aitchison, K.A., 1992. A Raman spectroscopic study of the initial stages of hydrolysis of tetraethoxysilane. *Mater. Res. Soc. Symp. Proc.* 271, 225–230.
- Box, G.E.P., Hunter, W.G., Hunter, J.S., 1978. In: *Statistics For Experimenters: An Introduction To Design, Data Analysis, and Model Building*, Wiley, New York.
- Chong, C.K., Shen, C., Fong, Y., Zhu, J., Yan, F.-X., Brush, S., Mann, C.K., Vickers, T.J., 1992. Raman spectroscopy with a fiber-optic probe. *Vib. Spectrosc.* 3, 35–45.
- Cooper, J.B., Philip E. Flecher, J., Welch, W.T., 1997. US Patent no. 5,684,580.
- Delgado-Lopez, M.M., 1997. Analytical Applications of Multichannel Raman. Ph. D. Thesis, The University of New Mexico, pp. 144.
- Dhanoa, M.S., Lister, S.J., Sanderson, R., Barnes, R.J., 1994. The link between multiplicative scatter correction (MSC) and standard normal variate (SNV) transformation of NIR spectra. *J. Near Infrared Spectrosc.* 2, 43–47.
- Farquharson, S., Simpson, S.F., 1992. Applications of Raman spectroscopy to industrial processes. *SPIE (Optically Based Methods for Process Analysis)* 1681, 276–290.
- Ford, J.F., Mann, C.K., Vickers, T.J., 1994. Monitoring the heterogeneously catalyzed conversion of quadricyclane to Norbornadiene by Raman spectroscopy. *Appl. Spectrosc.* 48, 592–595.
- Larsen, B.D., Christensen, D.H., Holm, A., Zillmer, R., Nielsen, O.F., 1993. The Merrifield peptide synthesis studied by near-infrared Fourier-transform Raman spectroscopy. *J. Am. Chem. Soc.* 115, 6247–6253.
- Marteau, P., Hotier, G., Zanier-Szydowski, N., Aoufi, A., Cansell, F., 1994a. Advanced control of C<sub>8</sub> aromatics separation process with real-time multipoint on-line Raman spectroscopy. *Process Control Quality* 6, 133–140.
- Marteau, P., Zanier, N., Aoufi, A., Hotier, G., Cansell, F., Silva, E.d., 1994b. Monitoring of an industrial process with remote Raman spectroscopy. *Analisis Mag.* 22, 32–34.
- Marteau, P., Zanier-Szydowski, N., Aoufi, A., Hotier, G., 1995. Remote Raman spectroscopy for process control. *Vib. Spectrosc.* 9, 101–109.
- Martens, H., Næs, T., 1989. In: *Multivariate Calibration*, Wiley, New York.
- Martin, M.Z., Garrison, A.A., Roberts, M.J., Hall, P.D., Moore, C.F., 1993. Composition monitoring by on-line remote Raman spectroscopy. *Process Control Quality* 5, 187–192.
- Nave, S.E., O'Rourke, P.E., Toole, W.R., 1995. Sampling probes enhance remote chemical analyses. *Laser Focus World* December, 83–88.
- Nelson, E.W., Scranton, A.B., 1996. Kinetics of cationic photopolymerizations of divinyl ethers characterized using In Situ Raman spectroscopy. *J. Polym. Sci. Part A: Polym. Chem.* 34, 403–411.
- Nomikos, P., MacGregor, J.F., 1994. Monitoring batch processes using multiway principal component analysis. *AIChE J.* 40, 1361–1375.
- Nomikos, P., MacGregor, J.F., 1995a. Multivariate SPC charts for monitoring batch processes. *Technometrics* 37, 41–59.
- Nomikos, P., MacGregor, J.F., 1995b. Multi-way partial least-squares in monitoring batch processes. *Chemom. Intell. Lab. Syst.* 30, 97–108.
- Pelletier, M.J., Davis, K.L., Carpio, R.A., 1996. Shining a light on wet process control. *Semiconductor Int.* March, 103–108.
- Purcell, F., Grayzel, R., Adar, F., 1992. Remote Raman analysis for process monitoring applications. *SPIE (Optically Based Methods for Process Analysis)* 1681, 149–158.
- Rice, S.F., Hunter, T.B., Rydén, Å.C., Hanush, R.G., 1996. Raman spectroscopic measurement of oxidation in supercritical water. 1. Conversion of methanol to formaldehyde. *Ind. Eng. Chem. Res.* 35, 2161–2171.
- Rännar, S., MacGregor, J.F., Wold, S., 1998. Adaptive batch monitoring using hierarchical PCA. *Chemom. Intell. Lab. Syst.* 41, 73–81.
- Schoppelrei, J.W., Kieke, M.L., Brill, T.B., 1996. Spectroscopy of hydrothermal reactions. 2. Reactions and kinetic parameters of (NH<sub>3</sub>OH)NO<sub>3</sub> and equilibria of (NH<sub>4</sub>)<sub>2</sub>CO<sub>3</sub> determined with a flow cell and FT Raman spectroscopy. *J. Phys. Chem.* 100, 7463–7470.
- Seasholtz, M.B., Archibald, D.D., Lorber, A., Kowalski, B.R., 1989. Quantitative analysis of liquid fuel mixtures with the use of Fourier transform near-IR Raman spectroscopy. *Appl. Spectrosc.* 43, 1067–1072.
- Shimoyama, M., Maeda, H., Matsukawa, K., Inoue, H., Ninomiya, T., Ozaki, Y., 1997. Discrimination of ethylene/vinyl acetate copolymers with different composition and prediction of the vinyl acetate content in the copolymers using Fourier-transform Raman spectroscopy and multivariate data analysis. *Vib. Spectrosc.* 14, 253–259.
- Svensson, O., Josefson, M., Langkilde, F.W., 1999. Reaction monitoring using Raman spectroscopy and chemometrics. *Chemom. Intell. Lab. Syst.* 49, 49–66.
- Thelin, B., Lundstedt, T., Lundgren, R., Olsson, A., Batra, S., 1995. Classification of Estradurin® batches: correlation between <sup>31</sup>P NMR and a biological duration test for batch approval. *Chemom. Intell. Lab. Syst.* 27, 135–145.
- Umetri AB. Manual SIMCA 7.0, (1998) Umetri AB, Umeå.
- van Staden, J.F., Makhafole, M.A., Waal, D.d., 1996. Kinetic study of the decomposition of nitrite to nitrate in acid samples using Raman spectroscopy. *Appl. Spectrosc.* 50, 991–994.
- Wang, C., Vickers, T.J., Schlenoff, J.B., Mann, C.K., 1992. In situ monitoring of emulsion polymerization using fiber-optic Raman spectroscopy. *Appl. Spectrosc.* 46, 1729–1731.
- Vess, T.M., Angel, S.M., 1992. Near-visible Raman instrumentation for remote multi-point process monitoring using fibers and optical multiplexing. *SPIE (Environmental and Process Monitoring Technologies)* 1637, 118–125.
- Vickers, T.J., Mann, C.K., 1992. Monitoring by fiber-optic Raman spectroscopy. *SPIE (Environmental and Process Monitoring Technologies)* 1637, 62–71.
- Williams, K.P.J., Aries, R.E., Cutler, D.J., Lidiard, D.P., 1990. Determination of gas oil cetane number and vetane index using near-infrared Fourier transform Raman spectroscopy. *Anal. Chem.* 62, 2553–2556.
- Wold, S., 1978. Cross-validatory estimation of the number of components in factor and principal components models. *Technometrics* 20, 397–405.
- Wold, S., Kettaneh, N., Fridén, H., Holmberg, A., 1998. Modelling and diagnostics of batch processes and analogous kinetic experiments. *Chemom. Intell. Lab. Syst.* 44, 331–340.
- Vorsina, I.A., Grishakova, T.E., Mikhailov, Y.I., 1995. Thermal decomposition of ammonium persulfate studied by Raman spectroscopy. *Inorg. Mater.* 31, 1321–1324.